Near Neutral pH Redox Flow Battery with Low Permeability and Long-Lifetime Phosphonated Viologen Active Species

Shijian Jin, Eric M. Fell, Lucia Vina-Lopez, Yan Jing, P. Winston Michalak, Roy G. Gordon,* and Michael J. Aziz*

A highly stable phosphonate-functionalized viologen is introduced as the redox-active material in a negative potential electrolyte for aqueous redox flow batteries (ARFBs) operating at nearly neutral pH. The solubility is 1.23 M and the reduction potential is the lowest of any substituted viologen utilized in a flow battery, reaching -0.462 V versus SHE at pH = 9. The negative charges in both the oxidized and the reduced states of 1,1'-bis(3-phosphonopropyl)-[4,4'-bipyridine]-1,1'-diium dibromide (BPP-Vi) effect low permeability in cation exchange membranes and suppress a bimolecular mechanism of viologen decomposition. A flow battery pairing BPP-Vi with a ferrocyanide-based positive potential electrolyte across an inexpensive, non-fluorinated cation exchange membrane at pH = 9 exhibits an open-circuit voltage of 0.9 V and a capacity fade rate of 0.016% per day or 0.00069% per cycle. Overcharging leads to viologen decomposition, causing irreversible capacity fade. This work introduces extremely stable, extremely low-permeating and low reduction potential redox active materials into near neutral ARFBs.

1. Introduction

The cost of renewable electricity from photovoltaics and wind has decreased significantly over the last four decades to the point that these clean resources have become realistic alternatives to fossil fuels for generating electricity. [1-3] However, unlike burning fossil fuels, which is easily tunable to meet human needs, wind and solar are unpredictable and intermittent due to day/night shift and seasonal changes, which hampers their penetration into the electrical grid. [4] The incorporation of safe, low-cost and large-scale energy storage into the electrical grid could solve this problem. [2] The most well-known and most widely applied grid-scale energy storage is pumped-hydro storage,

S. Jin, E. M. Fell, L. Vina-Lopez, Prof. R. G. Gordon, Prof. M. J. Aziz John A. Paulson School of Engineering and Applied Sciences Harvard University
Cambridge, MA 02138, USA
E-mail: gordon@chemistry.harvard.edu; maziz@harvard.edu
Dr. Y. Jing, Prof. R. G. Gordon
Department of Chemistry and Chemical Biology
Harvard University
Cambridge, MA 02138, USA
P. W. Michalak
Harvard College
Cambridge, MA 02138, USA
The ORCID identification number(s) for the author(s) of this article

can be found under https://doi.org/10.1002/aenm.202000100.

DOI: 10.1002/aenm.202000100

but its specific geographical requirement forestalls universal application, and concerns over ecosystem destruction limit its growth even in accommodating geographies. Other energy storage methods such as lithium-ion batteries, compressedair, and fuel cells share a limited portion of the energy storage market because of their high cost, safety concerns, limited discharge duration, low energy efficiency, or other difficulties.^[5] Aqueous redox flow batteries, possessing non-flammable electrolytes, decoupled energy/power scaling, and potential low cost, demonstrate strong potential for grid-scale energy storage. [6] Several MW/MWh sized all-vanadium flow batteries (VRFBs) have been installed across the globe. [7,8] However, widespread deployment of VRFBs is hindered by the high and volatile price of vanadium. Organic redox-active materials, composed

of earth-abundant elements such as C, H, O, N, S, and P, potentially have lower and more stable costs compared to vanadium. [9,10] Another unique benefit of organic molecules is their structural tunability, which enables various beneficial properties such as stability, solubility, proper redox potential, fast kinetics, and low toxicity to be pursued by the research community.

Quinones and viologens are among the most studied organic molecules for aqueous redox flow battery (ARFB) negolytes (negative electrolytes) because of their chemical stability and fast kinetics.^[11] Ionic or nonionic groups such as -SO₃-,^[12,13] $-O^{-}$, [14-16] $-COO^{-}$,[17,18] $-PO_3^{2-}$,[19] $-NR_3^{+}$,[20] and poly-ethylene glycol,[21] have been tethered to redox active cores to achieve reasonable solubilities in aqueous solutions. Quinones, though undergoing two-electron redox processes, are usually operable in extreme pH (pH = 0 or pH > = 12). [12,14,17] Recently, quinones soluble at near neutral pH (pH = 7-9) have been developed, but the electrolyte pH still swings considerably (up to pH = 13) due to proton coupled electron transfer during charging.[19,21] On the other hand, viologens are soluble at pH = 7 and their redox reactions do not involve coupled protons or hydroxides, thus maintaining stable pH during cycling. Therefore, viologen electrolytes can be less corrosive to electrolyte-contacting materials, which potentially reduces maintainance cost. Another advantage of having near neutral solution is the high stability and solubility of ferrocyanide, which is the most promising posolyte (positive electrolyte) in terms of stability.[11,17,22] First generation viologen-based flow batteries utilized methyl viologen (MV) electrolytes as active material. The high solubility of MV

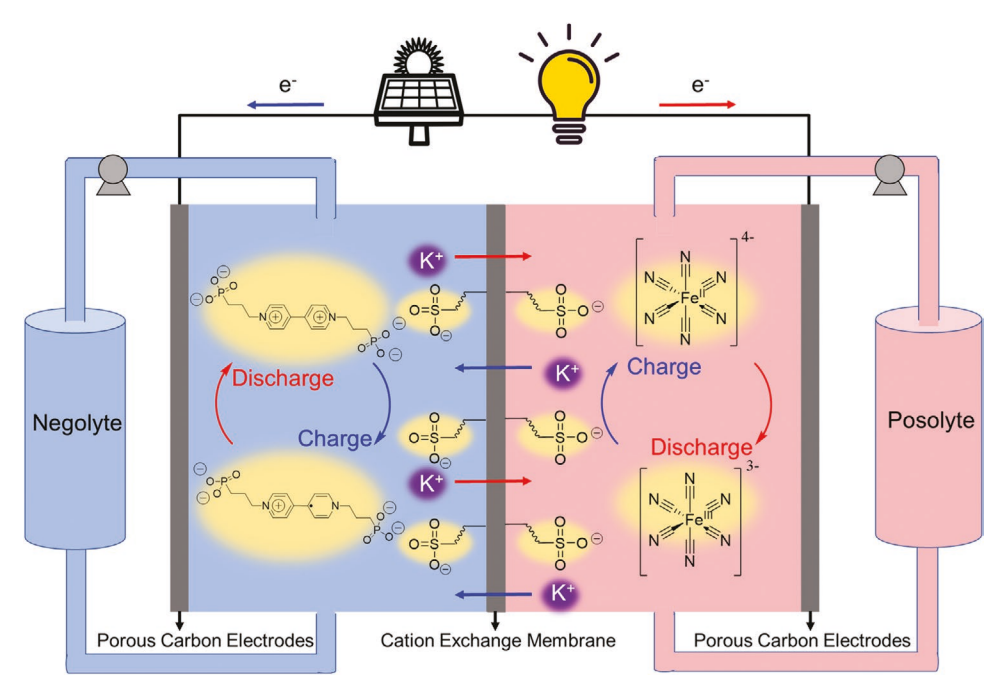


Figure 1. Scheme of BPP–Vi | ferrocyanide flow battery with enlarged reaction chamber. Negatively charged species are highlighted in yellow. Red arrows refer to a galvanic (discharging) process and blue arrows refer to an electrolytic (charging) process. Both the oxidized and the reduced forms of BPP–Vi are negatively charged, so they are repelled by the sulfonate-rich membrane, which minimizes BPP–Vi permeation.

in neutral pH solution and its fast kinetics, decent reduction potential (-0.45 V vs SHE, ≈0.9 V cell voltage when paired with ferrocene derivatives) and facile synthesis have been demonstrated by researchers.[18,23,24] However, MV-based flow batteries experience high capacity fade rates on the order of ≈1% per day, caused by both MV permeating through membranes and a bimolecular decomposition mechanism.^[20] Beh et al. addressed both of these issues by tethering trimethyl ammonium groups to the viologen core to make a +4 charged bis(3-trimethylammonio)propyl viologen tetrachloride (BTMAP-Vi).[20] The high number of positive charges enhances the repulsion among viologen molecules as well as the repulsion between viologen and the positively charged anion exchange membrane (AEM). However, the drawback is that the presence of electronwithdrawing trimethyl ammonium groups raises the reduction potential of BTMAP-Vi to -0.36 V versus SHE, causing lower cell voltage and low power density. DeBruler et al. have demonstrated a sulfonated viologen zwitterion 1,1'-bis(3sulfonatopropyl)-4,4'-bipyridinium ((SPr)2 V) that has a reduction potential of -0.43 V versus SHE and is compatible with cation exchange membranes (CEM) such as Nafion series and Selemion CSO, which have lower resistance than the AEMs used by Beh et al.[13] Pairing the (SPr)₂V based negolyte with (NH₄)₄Fe(CN)₆ or Br⁻ in a flow cell achieved power densities of 99^[25] and 227 mW cm⁻², ^[26] respectively. However, because of low charge in the oxidized (0 charge) and reduced state (-1 charge), (SPr)₂ V permeates through the CEM at a high rate.^[25] Although Luo et al. addressed this issue by putting (SPr)2 V on both sides of the CEM to balance the chemical potential, full material utilization was sacrificed, thus raising cost and lowering specific energy, and potentially creating complicating interactions among active species.^[20,25]

This work presents a phosphonate group-substituted viologen, i.e., 1,1'-bis(3-phosphonopropyl)-[4,4'-bipyridine]-1,1'diium (BPP-Vi), which has a -2 charge in the oxidized state and -3 charge in the reduced state at pH = 9. The negative charge makes BPP-Vi less susceptible to bimolecular decomposition and slows permeation through a CEM (Figure 1), compared with previously developed viologens. Pairing BPP-Vi with ferrocvanide and utilizing a cheap hydrocarbon-based Fumasep E620(K) CEM, our 1 м high BPP-Vi concentration full cell exhibits an open-circuit voltage (OCV) of ≈0.9 V and an extremely low capacity fade rate [11] of 0.016% per day or 0.00069% per cycle. No crossover of electroative material from either posolyte or negolyte was detected after extended cycling. A power density of 143 mW cm⁻² was achieved, which is 44% higher than that of previously demonstrated viologen|ferrocyanide cells.

2. Results and Discussion

BPP–Vi was synthesized through a simple S_N2 reaction, followed by a hydrolysis of the ester (**Scheme 1**). Each step was purified through simple filtration and the overall yield was 79% with high purity over the two steps (Figures S1–S2, Supporting Information). The facile synthesis and purification facilitate industrial large-scale production since neither catalyst nor resource-intensive chromatography are needed. Solubility of **BPP–Vi** was measured through UV–Vis spectrophotometry and the maximum solubility is 1.23 μ (Figure S4, Supporting Information). Titration (**Figure 2a**) of the 0.1 μ **BPP–Vi** solution shows that the pK_{a1} and pK_{a2} are the same as phosphonic acid, located at pH = 2 and pH = 7, respectively.

Scheme 1. Synthesis of BPP–Vi through substitution of diethyl (3-bromopropyl)phosphonate with 4,4'-bipyridine, followed by deprotection by bromotrimethylsilane.

Reaction kinetics of BPP-Vi were evaluated through cyclic voltammetry (CV) at different pH (Figure S6, Supporting Information). Figure 2b shows that the reduction potentials of the first and second redox pairs of BPP-Vi do not vary significantly with pH, which suggests that proton coupled electron transfer does not occur. The slight variation in reduction potential is caused by different buffer compositions and different degrees of phosphonate ionization. At slightly acidic pH, both redox processes of BPP-Vi are irreversible, signified by the small or non-existent oxidation peak (Figure S6. Supporting Information). At highly basic pH (pH = 14), the small side peak near -0.9 V versus SHE suggests that decomposition, i.e., cleavage of one of the alkyl chains, of BPP-Vi has occurred (Figure S6, Supporting Information). Reversible CV peaks were obtained over pH range 8.1-13.0, which aligns with the fully deprotonated region from the titration curve. At pH = 9, the reduction potential of **BPP-Vi** is -0.46 V versus SHE (Figure 2c), which will deliver a cell voltage of 0.9 V when paired with ferrocyanide, and this pH was used in further cell tests. Linear sweep voltammetry with a rotating disk electrode of a 5×10^{-3} M BPP–Vi solution was performed at pH = 9 and demonstrated a diffusion coefficient of 2.7×10^{-6} cm² s⁻¹ for the oxidized form and 2.6×10^{-6} cm² s⁻¹ for the singly reduced form (Figure S7, Supporting Information). The rate constant for the first and second reduction reactions were determined to be 2.9×10^{-3} and 2.2×10^{-3} cm s⁻¹, respectively (Figure S8–S9, Supporting Information).

To investigate the chemical and electrochemical stability of BPP-Vi, thermal stability tests and symmetric cell cycling of BPP-Vi were conducted. 0.1 M BPP-Vi solutions at pH = 9 were stored at 65 °C for one week. Proton nuclear magnetic resonance (¹H NMR) experiments conducted at the beginning and the end of the week revealed that the oxidized form of BPP-Vi is stable at the elevated temperature, which infers

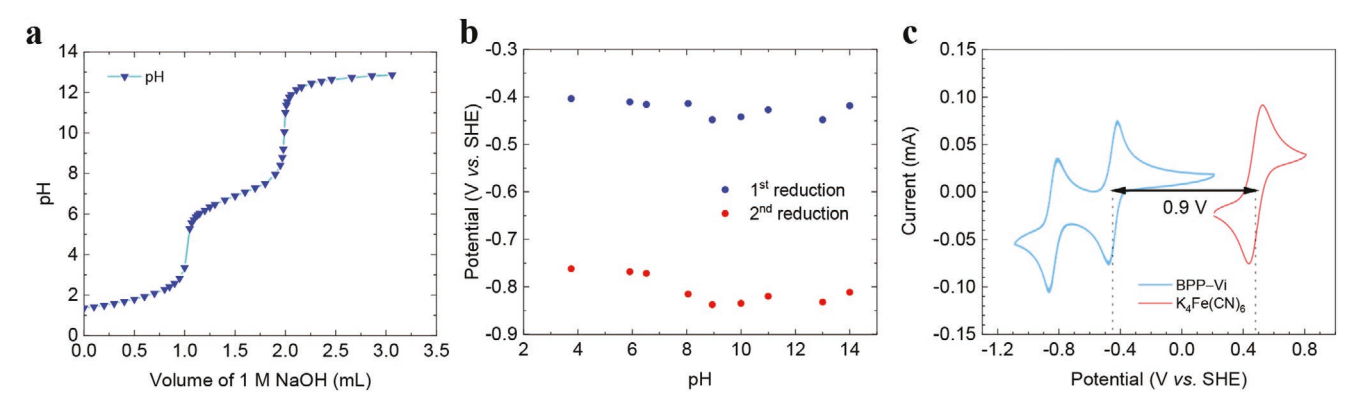


Figure 2. Characterization of BPP–Vi. a) Titration of 5 mL 0.1 M BPP–Vi with 1 M NaOH shows that the pK_{a1} of BPP–Vi is near pH = 2 and pK_{a2} is near pH = 7. b) The reduction potentials of both BPP–Vi redox reactions versus pH. The most negative reduction potential is achieved at pH = 9. c) Pairing BPP–Vi with K_4 Fe (CN) $_6$ at pH = 9 can lead to an equilibrium potential of 0.9 V.

www.advancedsciencenews.com www.advenergymat.de

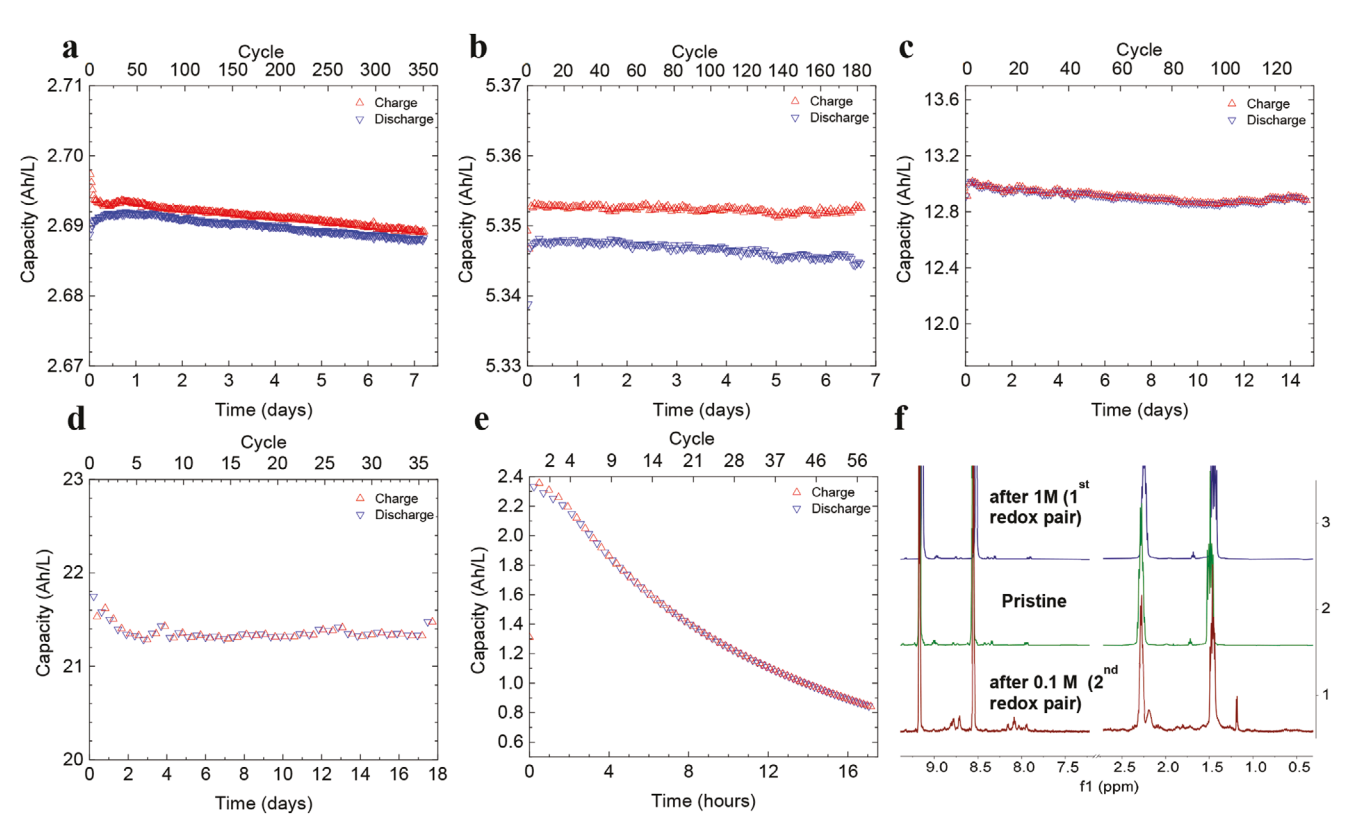


Figure 3. Volumetrically unbalanced compositionally symmetric cell cycling of BPP–Vi. The capacity limiting side has 6 mL of a) 0.1 м b) 0.2 м c) 0.5 м and d) 1 м BPP–Vi solution in 1 м KCl at pH = 9 and the non-capacity limiting side has 11 mL of the same concentration solution. Only the 1st (BPP–Vi²-/BPP–Vi³-) redox couple was accessed in a), b), c) and d). In e), only the 2nd (BPP–Vi³-/BPP–Vi³-) redox couple was accessed and the capacity decreased much more quickly. f) NMR spectra of BPP–Vi after cycling in d), pristine BPP–Vi, and BPP–Vi after e).

even higher chemical stability at lower temperature (Figure S5, Supporting Information). The stability of **BPP-Vi** in a battery was examined through potentiostatic cycling in a volumetrically unbalanced compositionally symmetric cell in a N2-filled glovebox. Several works have previously shown that symmetric cell cycling is a simple and efficient way to understand the chemical and electrochemical stability of flow battery reactants, because confounding factors such as reactants crossing over the membrane are suppressed.^[17,19,27] Cycling of 0.1 M BPP-Vi for 7 days and 350 cycles in a symmetric cell exhibited an extremely low fade rate of 0.014% per day or 0.0004% per cycle (Figure 3a). The cell was paused at the fully charged and fully discharged state for 4 and 2 days, respectively, and the temporal fading rate during these two periods was approximately equal to the cycling fading rate (Figure S12, Supporting Information). Symmetric cell cycling of 0.2 M BPP-Vi for 7 days and 0.5 M BPP-Vi for 16 days, exhibited fade rates of 0.0023% per day (0.0001% per cycle, Figure 3b) and 0.058% per day (0.0065% per cycle, Figure 3c), respectively; both fade rates are of the same order of magnitude as the rate at 0.1 м. For the 18-day symmetric cell cycling of 1 м ВРР-Vi, only 80% of the theoretical capacity was accessed due to high mass transport resistance, so the fading rate is inexplicable through cycling data (Figure 3d). However, ex situ chemical analysis, such as nuclear magnetic resonance (NMR) spectroscopy and liquid chromatography-mass spectrometry (LC-MS) did not show

any evidence of decomposition products (Figures S15–S19, Supporting Information).

The extensive symmetric cell cycling results are on par with previously reported fading rates of BTMAP-Vi.[27] In that work, the decomposition of methyl viologen (MV), which could be generalized to all viologen derivatives, is attributed to the dimerization of the reduced species, MV⁻⁺, followed by a disproportionation reaction that forms the oxidized species MV²⁺ and the doubly reduced species MV⁰, which can be protonated by water irreversibly to form a redox-inactive species. $\bar{\sl}^{[20,28]}$ DeBruler et al. presented results where two electrons are accessed during the cycling of 0.25 м BTMAP-Vi but the fading rate is 0.9% per day (0.01% per cycle), which is 9 times and 27 times faster than the fading in the cycling of 1.3 m and 0.75-1 m BTMAP-Vi, respectively, when only the first electron is accessed. [29] Both pieces of evidence suggest that accessing the doubly reduced species, either created through disproportionation or direct reduction, leads to instability. We wanted to determine whether BPP-Vi suffers the same fate. We name the oxidized form, singly reduced form and doubly reduced form of BPP-Vi to be BPP-Vi²⁻, BPP-Vi³⁻, and BPP-Vi⁴⁻, respectively. 20 mL 0.1 м BPP-Vi solution was charged to 50% state of charge (SOC) of the 2nd electron (50% BPP-Vi³⁻ and 50% BPP-Vi⁴⁻), and then 6 mL was used as the capacity limiting side (CLS) and 11 mL was used as the non-capacity limiting side (NCLS). The capacity faded by more than 60% within 17 h of cycling from 0% SOC

ENERGY

Table 1. Permeability of viologens through various membranes.

Molecule	Charge in the oxidized/ reduced form	Membrane	рН	Permeability [cm ² s ⁻¹]
MV ^{a)}	+2/+1	Selemion DSV AEM	7	3.4×10 ⁻⁹
BTMAP– Vi ^{a)}	+4/+3	Selemion DSV AEM	7	6.7×10^{-10}
(SPr) ₂ V	0/–1	N212 CEM	7	8.0×10^{-9}
(SPr) ₂ V	0/–1	E620 CEM	7	5.6×10^{-11}
BPP-Vi	-2/-3	N212 CEM	7	7.0×10^{-11}
BPP-Vi	-2/-3	E620 CEM	7	1.4×10^{-12}
BPP-Vi	-2/-3	N212 CEM	9	5.6×10^{-11}
BPP-Vi	-2/-3	E620 CEM	9	2.2×10^{-13}

a) Ref. [20].

to 100% SOC of the 2nd electron (Figure 3e). The NMR spectrum of the post-cycling solution shows primarily the original BPP-Vi²⁻ but some new peaks appear in both the aromatic and aliphatic regions (Figure 3f). The amount of decomposition product is significant. This result suggests a combination of apparent fading, possibly caused by auto-oxidation-induced imbalancing, and chemical decomposition, took place during the symmetric cell cycling of the BPP-Vi³⁻/BPP-Vi⁴⁻ pair. The molecular structure of the decomposition product is still under study, but the evidence clearly leads to the conclusion that accessing the second electron causes irreversible decomposition of BPP-Vi.

Based on the CV and the titration curve, the optimal electroactivity of BPP-Vi is achieved at pH near 9. We also expect a lower BPP-Vi permeability at pH = 9 compared to pH = 7because more BPP-Vi molecules are deprotonated at pH = 9, thus enhancing the repulsion between the membrane and the molecules. Debruler et al. show that a CEM can exclude (SPr)2 V through size-exclusion^[13] but Luo et al. show that material crossover still causes significant amounts of capacity fade — 2.6% per day in a full cell.^[25] Comparing the permeability of BPP-Vi and that of $(SPr)_2$ V using Nafion 212 as the test membrane at pH = 7, we find that **BPP–Vi** permeates at 7.1×10^{-11} cm² s⁻¹, which is two orders of magnitude slower than $(SPr)_2 V$, at $7.8 \times 10^{-9} \text{ cm}^2 \text{ s}^{-1}$ (Figure S11, , Supporting Information; Table 1). At pH = 9. the permeability of BPP-Vi is even lower, with a rate of 4.1×10^{-11} cm² s⁻¹ (Figure S11, Supporting Information), validating our hypothesis. We also implemented an inexpensive hydrocarbon-based membrane, Fumasep E620(K), which was proven to suppress the permeation of anthraquinones and ferro/ ferricyanide very well.^[17,19] The permeability of ferricyanide, the more permeating species of the pair, is 4.4×10^{-12} cm² s⁻¹ across $E620(K)^{[17]}$ and 4.5×10^{-9} cm² s⁻¹ across Nafion 212.^[30]The permeability of **BPP-Vi** through E620(K) is 1.4×10^{-12} cm² s⁻¹ at pH = 7 and 5.4×10^{-13} cm² s⁻¹ at pH = 9, which are both slower than the permeability through Nafion 212 (Figure S11, Supporting Information) (Table 1). With the lowest permeability value $(5.4 \times 10^{-13} \text{ cm}^2 \text{ s}^{-1})$, it should take 910 and 6000 years to lose 10% and 50% capacity, respectively, due to BPP-Vi crossover (Table S1), assuming exponential behavior.^[20] Figure S13 in

the Supporting Information demonstrated that E620(K) has a higher ionic conductivity at near neutral condition compared to Nafion 212. Therefore, full cell polarization and cycling experiments were conducted with E620(K) membrane at pH = 9.

Given the high chemical and electrochemical stability and low permeability through E620(K) membrane, BPP-Vi, paired with K₄Fe(CN)₆, was evaluated in full cells with E620(K) being the membrane at pH = 9. A 0.1 M concentration cell was charged at 10 mA cm⁻² and polarization curves were measured at 10% SOC intervals. The open-circuit voltage (OCV) increased from 0.89 V at 10% SOC to 1.0 V at 90% SOC, and the OCV at 50% SOC was 0.94 V (Figure 4a). The alternating current area-specific resistance (AC-ASR) of the cell was determined via high-frequency electrochemical impedance spectroscopy (EIS) and the value was slightly above 1 Ω cm² across all SOCs (Figure 4a). The proximity of the polarization resistance curve, which shows the value of direct current area-specific resistance (DC-ASR), and the high frequency resistance curve shows that more than 60% of the resistance of the cell can be attributed to the membrane resistance (Figure 4a). A peak power density of 0.145 W cm⁻² was observed at 100% SOC and the value at 50% SOC is 0.123 W cm⁻² (Figure 4b). High coulombic efficiency was realized at all current densities, thus the loss in energy efficiency is attributed to voltage efficiency, which is expected to increase when membrane resistance is lowered (Figure 4c,d). Only 30% of the capacity can be accessed at 100 mA cm⁻² because a low voltage cutoff (1.1 V) was chosen to avoid accessing the 2nd electron (Figure 4d, see below for further details).

A flow cell with 6 mL of 0.1 m BPP-Vi negolyte and 20 mL of 0.1 м K₄Fe(CN)₆/0.04 м K₃Fe(CN)₆ posolyte was placed in a N₂filled glovebox for an extended cycling study. The small amount of ferricyanide prevents the posolyte from becoming the capacity limiting side during discharge in case it undergoes slow reductive side reactions at high SOC; this precaution permits us to focus our attention only on the stability of the negolyte. The cell was first charged at 40 mA cm⁻² with 1.2 V cutoff during charge and 0.4 V cutoff during discharge. A 2 mA cm⁻² current cutoff to a potentiostatic hold was imposed as soon as the voltage cutoffs were reached. The capacity fade rate under such conditions was 0.2% per day or 0.00068% per cycle (Figure 4e). After 500 cycles, the charging voltage cutoff was set to 1.1 V while maintaining other conditions. The capacity fade rate became 0.019% per day or 0.00013% per cycle across 4 days and 500 cycles (Figure 4e points B to C). Once the charging voltage cutoff was set to 1.2 V again, the fade rate increased by more than one order of magnitude. The cell was then cycled with 1.1 V charging voltage cutoff for 16 days or 2300 cycles. A 0.024% per day or 0.00017% per cycle capacity fade rate was maintained (Figure 4e points F to G). We increased the voltage cutoff for charge at the end of the cycling in order to check whether the fade rate was real. The capacity difference between points A and D, and that between points E and H, are consistent with the difference between points B and C, and the difference between points F and G, respectively (Figure 4e). Such consistency demonstrates that the ≈0.02% per day fading rate is real. We suspect the higher fading rate at higher voltage cutoff is due to partial access of the second electron reduction. Theoretically, according to the Nernst equation with dilute solution assumptions, neglecting ohmic, kinetic, and mass-transport

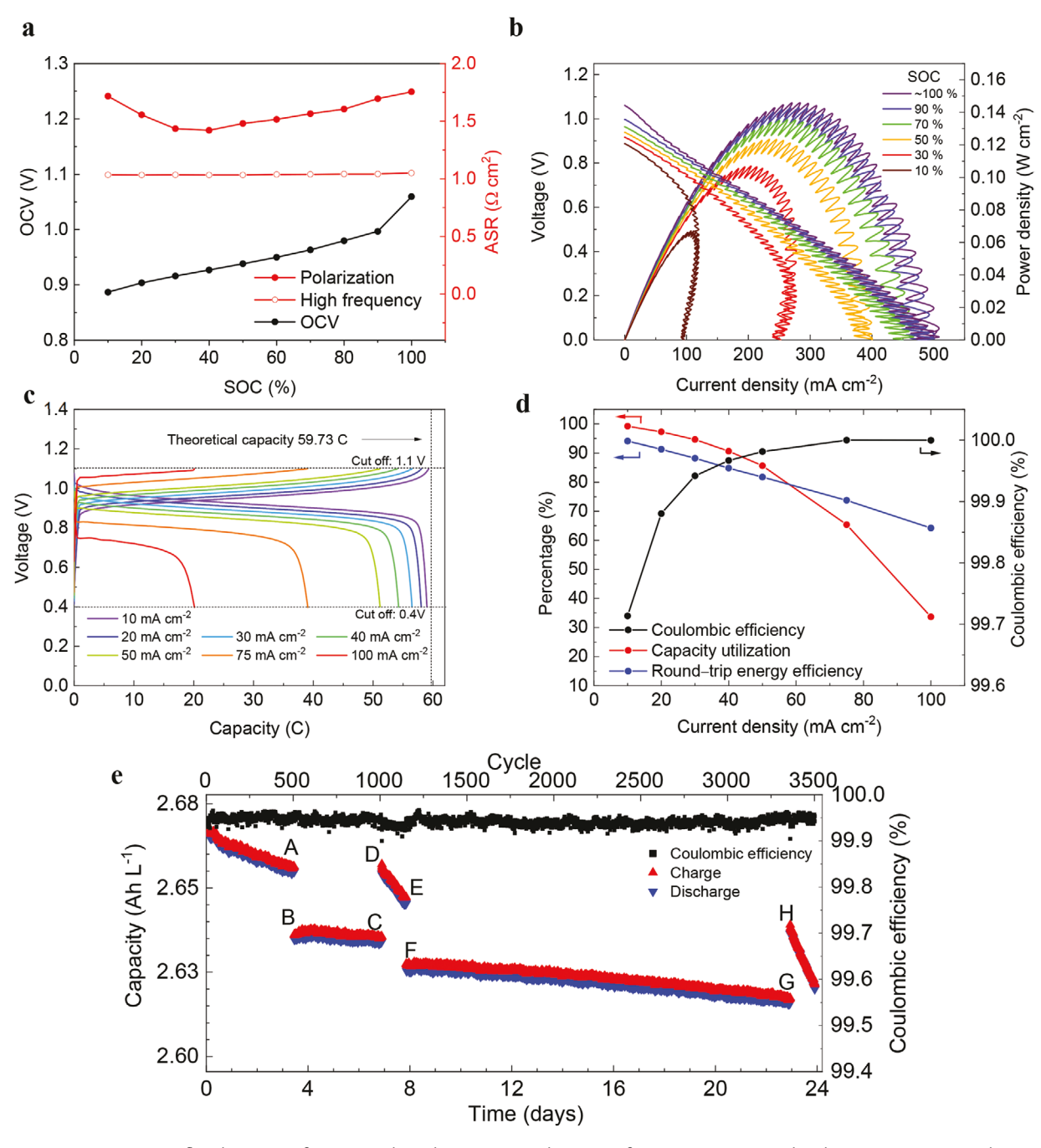


Figure 4. Low-concentration flow battery performance. Electrolytes comprised 6.2 mL of 0.1 m BPP–Vi titrated with 1 m KOH in 1 m KCl to pH = 9 (negolyte) and 20 mL of 0.1 m K_4 Fe(CN)₆ and 0.1 m K_3 Fe(CN)₆ in 1 m KCl at pH = 9 (posolyte). a) OCV, high frequency and polarization ASR versus SOC. b) Cell voltage and power density during discharge at various SOC. Oscillations arise from peristaltic pumping. c) Galvanostatic charge and discharge curves at various current densities with 1.1 and 0.4 V cutoffs. The theoretical capacity is indicated by the vertical dashed line. d) Coulombic efficiency, capacity utilization and round-trip energy efficiency versus current density. e) Extended cycling at 40 mA cm⁻² of the flow cell with same voltage cutoff for discharge (0.4 V) but different voltage cutoffs for charge. The voltage cutoff is 1.2 V for the periods, beginning to A, D to E, and H to the end. The voltage cutoff is 1.1 V for the periods B to C, and F to G. Stable cycling was observed when the lower charging cutoff was applied.

overpotentials, the accessible 2nd electron capacity is 47 times higher when 1.2 V is used compared to 1.1 V. The redox potential of the BPP–Vi³–/BPP–Vi⁴– couple is 400 mV lower than that of BPP–Vi²–/BPP–Vi³–, so we assume that the OCV of 50% SOC BPP–Vi³–/BPP–Vi⁴– versus K_4 Fe(CN)₆/ K_3 Fe(CN)₆ is 400 mV higher, i.e., 1.28 V. According to the Nernst equation

$$E = E^{\circ} - \frac{RT}{nF} \ln \frac{a_{BPP-V^{3-}} a_{[Fe(CN)_{6}]^{4-}}}{a_{BPP-V^{4-}} a_{[Fe(CN)_{6}]^{3-}}}$$
(1)

where E is the cell potential, E° is the cell OCV at 50% SOC, R is the universal gas constant, T is the absolute temperature (298 K),



n is the number of electrons transferred (1), F is the Faraday constant and a refers to the activity of each species. Assuming dilute solution conditions implies

$$\frac{a_{BPP-Vi^{3-}}}{a_{BPP-Vi^{4-}}} = \frac{C_{BPP-Vi^{3-}}}{C_{BPP-Vi^{4-}}} \quad \text{and} \quad \frac{a_{[Fe(CN)_6]^{4-}}}{a_{[Fe(CN)_6]^{3-}}} = \frac{C_{[Fe(CN)_6]^{4-}}}{C_{[Fe(CN)_6]^{3-}}}$$
(2)

where *C* refers to the concentration of each species. After the full reduction of **BPP-Vi**²⁻ to **BPP-Vi**³⁻, accompanied by oxidation of ferrocyanide to ferricyanide, the concentration of posolyte species changes to the following

$$C_{[Fe(CN)_6]^{4-}} = \frac{(0.02L \times 0.1M) - (0.006 L \times 0.1M)}{0.02L} = 0.07M$$
 (3)

$$C_{[Fe(CN)_6]^{3-}} = \frac{(0.02L \times 0.1M) + (0.006L \times 0.1M)}{0.02L} = 0.07M$$
 (4)

When the applied potential E is 1.1 V, assuming E° is 1.28 V, using equations Equation (1) to Equation (4), and applying the constraint

$$C_{BPP-Vi^{3-}} + C_{BPP-Vi^{4-}} = 0.1 M ag{5}$$

we deduce that $C_{BPP-Vio^{4-}}=0.00009\,M$ and $C_{BPP-Vio^{3-}}=0.09991\,M$. So the accessible BPP-Vi4 amount is around 0.009%. When 1.2 V is applied, using the same equations, 0.42% BPP-Vi⁴ can be accessed, which is 47 times higher than the accessed amount when 1.1 V is applied. The actual accessed percentage of BPP-Vi⁴⁻ is likely less than these amounts due to different types of overpotentials from DC-ASR at the currect cutoff value of 2 mA cm⁻², but the calculation shows that a significantly larger amount of BPP-Vi⁴⁻ is created when 1.2 V is applied. It is not very surprising that overcharging can cause capacity fade, as previous work shows that overcharging of anthraquinone, forming anthrone, is the dominant cause of capacity fade in an anthraquinone based flow battery.[31] We hypothesize that the fast degradation of the doubly reduced BPP-Vi4-, which is consistent with the symmetric cell cycling of the BPP-Vi³⁻/BPP-Vi⁴⁻ couple shown in Figure 4e, is the major source of capacity fade in all of our cells. To exploit the high solubility of BPP-Vi, we constructed a full cell with a concentrated negolyte comprising 5 mL 1.0 м BPP-Vi as the capacity-limiting side and posolyte comprising 20 mL of 0.5 M K₄Fe(CN)₆ /0.5 M Na₄Fe(CN)₆ with 0.1 M K₃Fe(CN)₆ as the non-capacity-limiting side. Over the 32 days of cell operation, we cannot report a conclusive fade rate because of the fluctuating capacity and the low accessed capacity (Figure S14, Supporting Information). We identify two potential reasons for the low accessed capacity: 1. the titration of saturated BPP-Vi with 10 м КОН, which may cleave the C-N bond of BPP-Vi and 2. the decomposition product clogging electrodes, which raises cell resistance. To avoid the issue caused by titration with strong base, a milder base, NH₄OH, was used. Even at 14 M, the ammonium hydroxide solution has a pH around 12. Indeed > 99.5% capacity utilization (Figure 5c,d) was achieved in a cell with 6.2 mL 1 м BPP-Vi tirated with NH₄OH as negolyte and 40 mL 0.3 м K₄Fe(CN)₆/0.3 м K₃Fe(CN)₆ in 2 м NH₄Cl as posolyte during galvanostatic cycling with potentiostatic holds at the

end. A 5 mA cm⁻² current cutoff to a potentiostatic hold was imposed as soon as the voltage cutoffs were reached. Although the AC-ASR was higher due to low water activity in the membrane, polarization experiments across 10% to 90% SOC do not exhibit higher DC-ASR compared to the low concentration case (Figure 5a). The OCV at 50% SOC is 0.88 V, which is slightly lower than that of the 0.1 m cell and is likely influenced by a subtle effect of different supporting electrolytes. The peak power was achieved at 100% SOC with a value of 0.143 W cm⁻² (Figure 5b). Galvanostatic cycling from 10 to 150 mA cm⁻² show that close to 80% capacity utilization and 70% round trip energy efficiency can be realized at 100 mA cm⁻² (Figure 5c,d). The extended cycling of this cell demonstrates a fade rate of 0.016% per day or 0.00069% per cycle (Figure 5e). When pairing with an equivalent volume of 1 m ferrocyanide, either with mixed K⁺/Na⁺ or NH₄⁺ counterion, the BPP-Vi based flow cell should have an energy density of 11.8 Wh L⁻¹. Thus, this flow battery chemistry is operable at pH = 9 with extremely high electrolyte stability, extremely low electrolyte permeation, and reasonable power and energy densities.

The reduction potential of **BPP-Vi** at pH = 9 is 100 mV more negative than that of BTMAP-Vi and 10 mV more negative than that of MV (Figure S20, Supporting Information). Yet the extremely high cycling stability of the BPP-Vi full cell is on par with that of the BTMAP-Vi cell, and their capacity fade rates are two order of magnitude lower than that of a MV cell. The coexistence of low reduction potential and high stability in viologens is encouraging because this is an attribute that appears to be lacking in anthraquinones. Goulet, Tong et al. demonstrated that anthraquinones with lower reduction potential are more susceptible to irreversible decomposition through anthrone/ bianthrone formation.[31] Although the decomposition mechanism of viologens is still under study, the absence of potentialstability correlation in such species suggests there are opportunities for developing a stable viologen with reduction potential close to the solvent stability window.

Although BPP-Vi has the most negative reduction potential among all viologen derivatives applied in aqueous flow batteries to date, the cell voltage is relatively low compared to many other flow batteries, including vanadium, phenazine, and some quinone-based chemistries.[11] Several directions are under study to raise the cell voltage of viologen-based flow batteries. For example, several groups have used (2,2,6,6-Tetramethylpiperidin-1-yl)oxyl or (2,2,6,6-tetramethylpiperidin-1-yl)oxidanyl (TEMPO) as posolyte.[18,24,29] We designed 4,4'-(3-sulfopropyl) amino)-(2,2,6,6-Tetramethylpiperidin-1-yl)oxyl (S-TEMPO), employing the same multi-negative charge concept as BPP-Vi; pairing S-TEMPO with BPP-Vi gives a potential difference of 1.3 V (Figure S10, Supporting Information). The cell performance of this pair is under study. Another method to further raise the cell potential is to further decrease the reduction potential of viologens. While the focus of our present work has been the development and performance of BPP-Vi, we additionally present preliminary results on 2,2'-methyl-substituted viologen species, illustrating substitutions that can further lower the reduction potential of viologens. Figure 6a-c shows that the 2,3'-dimethyl-1,1'-bis(3-phosphonopropyl)-[4,4'-bipyridine]-1,1'-diium dibromide (BPP-mVi), 3,3'-(2,3'-dimethyl-[4,4'bipyridine]-1,1'-diium-1,1'-diyl)bis(propane-1-sulfonate)

www.advenergymat.de

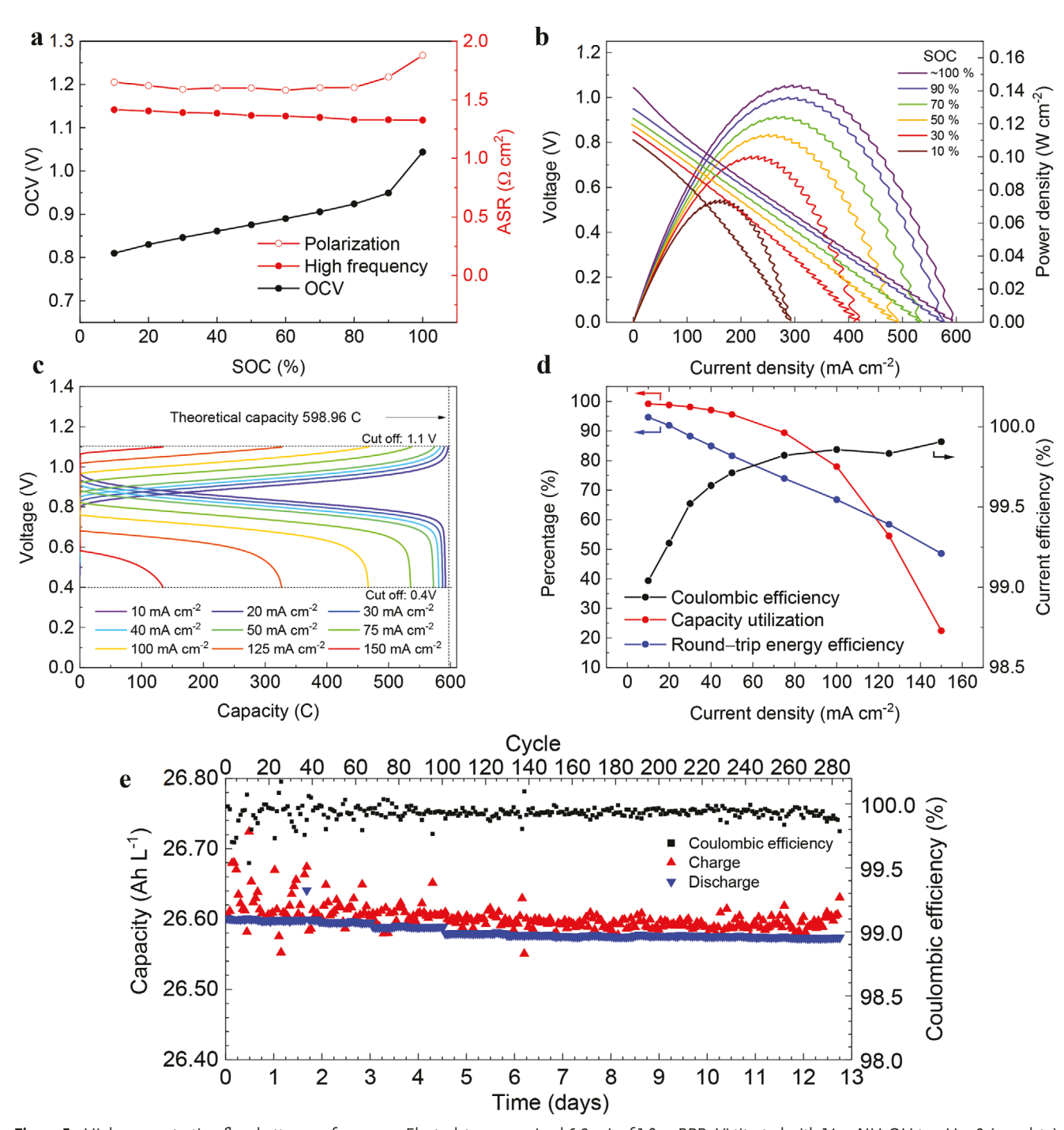


Figure 5. High-concentration flow battery performance. Electrolytes comprised 6.2 mL of 1.0 m BPP–Vi titrated with 14 m NH₄OH to pH = 9 (negolyte) and 40 mL of 0.3 m K_4 Fe(CN)₆ and 0.3 m K_3 Fe(CN)₆ in 2 m NH₄Cl at pH = 9 (posolyte). a) OCV, high frequency and polarization AC-ASR versus SOC. b) Cell voltage and power density during discharge at various SOC. c) Galvanostatic charge and discharge curves at various current densities with 1.1 and 0.4 V cutoffs. The theoretical capacity is indicated by the vertical dashed line. d) Coulombic efficiency, capacity utilization and round trip energy efficiency versus current density. e) Extended cycling at 40 mA cm⁻² of the flow cell with 1.1 V charging voltage.

(BPS-mVi), and 2,2'-dimethyl-1,1'-bis(3-(trimethylammonio) propyl)-[4,4'-bipyridine]-1,1'-diium tetrabromide (BTMAP-mVi), have reduction potentials that are 86, 77, and 95 mV, respectively, more negative than the corresponding unsubstituted molecules at pH = 8. Such modifications can increase the overall cell voltage by \approx 10%, with corresponding increases

in energy density and power density. Computational results show that when stronger electron-donating groups, such as methoxy groups, are installed, the reduction potential may be further lowered (Figure S20, Supporting Information). These developments, in light of the absence of the unfavorable potential-stability correlation in viologen derivatives, may lead

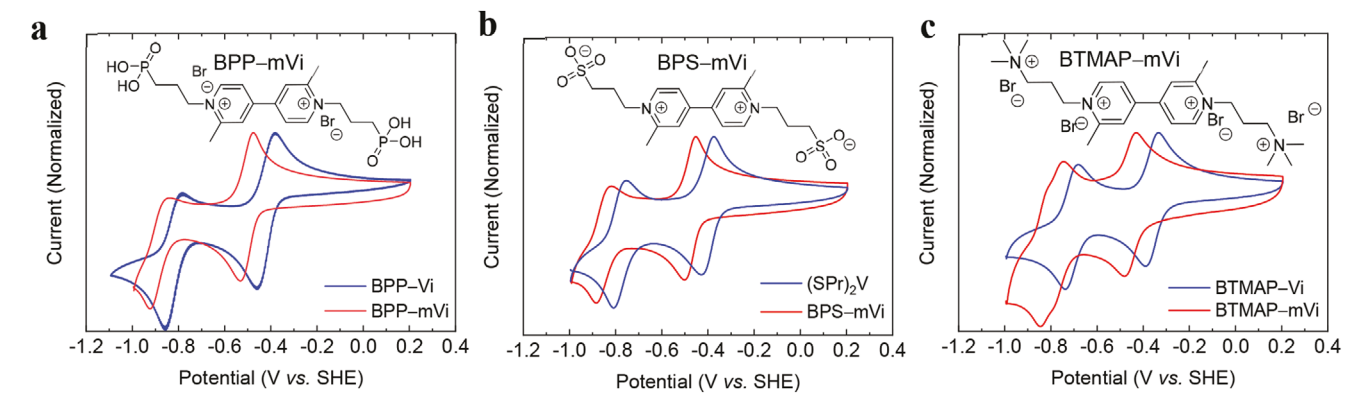


Figure 6. Comparison of CV of 2.2'-methylated funtionalized viologens and un-methylated viologens measured at pH = 8. The functional groups are 3-phosphonopropyl, propane-1-sulfonate and 3-(trimethylammonio) propyl in a), b) and c), respectively.

to higher-voltage ARFBs operating at near-neutral pH with the decadal lifetimes required for deployment on the grid.

Emily Kerr, Min Wu, Daniel Pollack, Dr. Andrew Wong, Dr. Zhijiang Tang, Dr. Yunlong Ji, Dr. Diana De Porcellinis, and Ziang Xu for useful discussions

3. Summary

We introduce BPP-Vi as a negolyte material for an ARFB that remains at near neutral pH throughout its charge-discharge cycle. The molecule is soluble up to 1.23 м and its reduction potential at pH = 9 of -0.462 V versus SHE is the most negative among viologens employed in flow batteries. The negative charges on both the oxidized and reduced forms of BPP-Vi help increase molecular stability and reduce permeation rates by enhancing electrostatic repulsion among BPP-Vi molecules and between molecules and the CEM. The measured permeability of BPP-Vi through a Fumasep E620 CEM is 2.2×10^{-13} cm² s⁻¹, which would result in $\approx 10\%$ capacity fade due to BPP-Vi crossover in 1000 years. A symmetric cell at 0.2 м BPP-Vi and a full cell at 1 м BPP-Vi demonstrate extremely low capacity fade rates of 0.0023% per day and 0.016% per day, respectively. Capacity fade rate experiments and post-mortem NMR measurements support the interpretation that capacity decay occurs if one accesses a chemically unstable doubly reduced form. The high-concentration full cell exhibits a peak power density of 0.14 W cm⁻² and a theoretical energy density of 11.8 W h L⁻¹, which might be further increased with the installation of electron donating groups on 2,2' positions on the viologen core. This work introduces extremely stable, extremely low-permeating and low reduction potential redox active materials into near neutral ARFBs.

Supporting Information

Supporting Information is available from the Wiley Online Library or from the author.

Acknowledgements

This research was supported by U.S. DOE award DE-AC05-76RL01830 through PNNL subcontract 428977, NSF grant CBET-1914543, and by the Massachusetts Clean Energy Technology Center. The authors thank

Conflict of Interest

The authors declare no conflict of interest.

Keywords

low permeability, neutral pH, redox flow batteries, viologen

Received: January 10, 2020 Revised: March 2, 2020 Published online: April 6, 2020

- [1] T. Stehly, D. Heimiller, G. Scott, National Renewable Energy Laboratory 2017.
- [2] P. Denholm, E. Ela, B. Kirby, M. Milligan, National Renewable Energy Laboratory 2010.
- [3] B. Obama, Science 2017, 355, 126.
- [4] J. Rugolo, M. Aziz, Energy Environ. Sci. 2012, 5, 7151.
- [5] B. Dunn, H. Kamath, J.-M. Tarascon, Science 2011, 334, 928.
- [6] J. Luo, B. Hu, M. Hu, Y. Zhao, T. L. Liu, ACS Energy Lett. 2019, 4,
- [7] https://electrek.co/2017/12/21/worlds-largest-battery-200mw-800mwh-vanadium-flow-battery-rongke-power/, "World's Largest Battery: 200MW/800 MWh Vanadium Flow Battery - Site Work Ongoing," accessed.
- [8] https://global-sei.com/company/press/2018/12/prs102.html, accessed 2019/12/07.
- [9] J. Winsberg, T. Hagemann, T. Janoschka, M. D. Hager, U. S. Schubert, Angew. Chem., Int. Ed. 2017, 56, 686.
- [10] G. L. Soloveichik, Chem. Rev. 2015, 115, 11533.
- [11] D. G. Kwabi, Y. Ji, M. J. Aziz, Chem. Rev. 2020, https://doi. org/10.1021/acs.chemrev.9b00599.
- [12] B. Huskinson, M. P. Marshak, C. Suh, S. Er, M. R. Gerhardt, C. J. Galvin, X. Chen, A. Aspuru-Guzik, R. G. Gordon, M. J. Aziz, Nature 2014, 505, 195.
- [13] B. Hu, C. DeBruler, J. Moss, J. Luo, T. L. Liu, ACS Energy Lett. 2018,



ENERGY MATERIALS

www.advancedsciencenews.com www.advenergymat.de

- [14] K. Lin, Q. Chen, M. R. Gerhardt, L. Tong, S. B. Kim, L. Eisenach, A. W. Valle, D. Hardee, R. G. Gordon, M. J. Aziz, M. P. Marshak, Science 2015, 349, 1529.
- [15] L. Tong, M.-A. Goulet, D. P. Tabor, E. F. Kerr, D. De Porcellinis, E. M. Fell, A. Aspuru-Guzik, R. G. Gordon, M. J. Aziz, ACS Energy Lett. 2019, 4, 1880.
- [16] Z. J. Yang, L. C. Tong, D. P. Tabor, E. S. Beh, M. A. Goulet, D. De Porcellinis, A. Aspuru-Guzik, R. G. Gordon, M. J. Aziz, Adv. Energy Mater. 2018, 8, 1702056.
- [17] D. G. Kwabi, K. Lin, Y. Ji, E. F. Kerr, M.-A. Goulet, D. De Porcellinis, D. P. Tabor, D. A. Pollack, A. Aspuru-Guzik, R. G. Gordon, M. J. Aziz, *Joule* 2018, 2, 1907.
- [18] T. Janoschka, N. Martin, M. D. Hager, U. S. Schubert, Angew. Chem., Int. Ed. 2016, 55, 14427.
- [19] Y. Ji, M. A. Goulet, D. A. Pollack, D. G. Kwabi, S. Jin, D. Porcellinis, E. F. Kerr, R. G. Gordon, M. J. Aziz, Adv. Energy Mater. 2019, 9, 1900039.
- [20] E. S. Beh, D. De Porcellinis, R. L. Gracia, K. T. Xia, R. G. Gordon, M. J. Aziz, ACS Energy Lett. 2017, 2, 639.
- [21] S. Jin, Y. Jing, D. G. Kwabi, Y. L. Ji, L. C. Tong, D. De Porcellinis, M. A. Goulet, D. A. Pollack, R. G. Gordon, M. J. Aziz, ACS Energy Lett. 2019, 4, 1342.

- [22] J. Luo, A. Sam, B. Hu, C. DeBruler, X. L. Wei, W. Wang, T. L. Liu, Nano Energy 2017, 42, 215.
- [23] B. Hu, C. DeBruler, Z. Rhodes, T. L. Liu, J. Am. Chem. Soc. 2017, 139, 1207.
- [24] T. B. Liu, X. L. Wei, Z. M. Nie, V. Sprenkle, W. Wang, Adv. Energy Mater. 2016, 6, 1501449.
- [25] J. Luo, B. Hu, C. Debruler, Y. J. Bi, Y. Zhao, B. Yuan, M. W. Hu, W. D. Wu, T. L. Liu, *Joule* 2019, 3, 149.
- [26] J. Luo, W. D. Wu, C. Debruler, B. Hu, M. W. Hu, T. L. Liu, J. Mater. Chem. A 2019, 7, 9130.
- [27] M. A. Goulet, M. J. Aziz, J. Electrochem. Soc. 2018, 165, A1466.
- [28] M. Venturi, Q. G. Mulazzani, M. Z. Hoffman, Radiat. Phys. Chem. 1984, 23, 229.
- [29] C. DeBruler, B. Hu, J. Moss, X. A. Liu, J. A. Luo, Y. J. Sun, T. L. Liu, Chem 2017, 3, 961.
- [30] D. De Porcellinis, B. Mecheri, A. D'Epifanio, S. Licoccia, S. Granados-Focil, M. J. Aziz, J. Electrochem. Soc. 2018, 165, A1137.
- [31] M. A. Goulet, L. Tong, D. A. Pollack, D. P. Tabor, S. A. Odom, A. Aspuru-Guzik, E. E. Kwan, R. G. Gordon, M. J. Aziz, J. Am. Chem. Soc. 2019, 141, 8014.